Materials Advances

ROYAL SOCIETY OF CHEMISTRY

PAPER

View Article Online
View Journal | View Issue

Cite this: *Mater. Adv.*, 2021, 2, 4081

Adsorbed xenon propellant storage: are nanoporous materials worth the weight?†

Melanie T. Huynh,[a] Nickolas Gantzler,[b] Samuel Hough,[a] David Roundy,[b] Praveen K. Thallapally[c] and Cory M. Simon*[a]

Xenon is used as a propellant for spacecraft. Conventionally, xenon is compressed to high pressures (75–300 bar) for bulk storage onboard the spacecraft. An adsorbed xenon storage system based on nanoporous materials (NPMs) could, potentially, (i) reduce the storage pressures, (ii) allow for thinner-walled and lighter pressure vessels, and (iii) if the NPM itself is sufficiently light, reduce the overall mass of the storage system and, thus, of the payload of the rocket launch. To investigate, we develop a simple mathematical model of an adsorbed xenon storage system by coupling a mechanical model for the pressure vessel and a thermodynamic model for the density of xenon adsorbed in the NPM. From the model, we derive the optimal storage pressure, tailored to each NPM, with the objective of minimizing the mass of the materials (walls of the pressure vessel + NPM) required to store the xenon. The model enables us to: (i) rank NPMs for adsorbed xenon propellant storage, (ii) compare adsorbed storage to the baseline of bulk storage, and (iii) understand what properties of NPMs are desirable for adsorbed xenon propellant storage. We use the model to evaluate several NPMs, mostly metal–organic frameworks (MOFs), for adsorbed xenon propellant storage at room temperature, using experimental xenon adsorption data as input. We find Ni-MOF-74 and MOF-505 outperform activated carbon, a traditional adsorbent. However, each optimized adsorbed xenon storage system is heavier than the optimized bulk storage system, owing dominantly to the large mass of the NPM itself. To provide a lighter adsorbed xenon storage system than a bulk storage system, our model suggests to pursue light adsorbents with a high gravimetric saturation loading of xenon.

Received 26th February 2021,
Accepted 12th May 2021

DOI: 10.1039/d1ma00167a

rsc.li/materials-advances

1 Introduction

Ion thrusters are used to propel spacecraft and satellites.[1,2] Xenon is commonly used as a propellant owing to its inertness, high molecular weight, and relatively low ionization energy.[3]

To store xenon propellant onboard the spacecraft, xenon is typically compressed and stored at high pressures (75–300 bar)[4–7] between 20 °C and 50 °C, in a supercritical state.[8] The pressure vessel must have thick walls to safely contain the xenon at these high pressures, making it heavy. Because the cost of launching a payload into Earths orbit is *ca.* 10 000 USD per lb,[9] it is desirable to reduce the mass of storage materials required to store xenon propellant onboard spacecraft.

We investigate the feasibility of an alternative xenon storage strategy, with the objective of reducing the mass of the storage materials required to carry the xenon propellant into space: packing the pressure vessel with a porous adsorbent material to help densify the xenon (*i.e.*, use an adsorbent in combination with pressurization). Activated carbon has been investigated for adsorbed xenon propellant storage, but it does not reduce the mass of the storage system.[10] Newer classes of nanoporous materials, such as metal–organic frameworks (MOFs),[11] porous organic cages (POCs),[12] and covalent organic frameworks (COFs),[13] exhibit very high internal surface areas[14,15] and have demonstrated promise for gas densification in the context of vehicular hydrogen and methane storage,[16] motivating us to consider these advanced nanoporous materials for adsorbed xenon propellant storage. Moreover, several of these nanoporous materials exhibit a high affinity for xenon, evidenced by their adsorptive selectivity for xenon in the context of separations.[17–20]

Herein, we develop a simple mathematical model of an adsorbed xenon propellant storage system by coupling a mechanical stress model for the pressure vessel and a thermodynamic model for gas adsorption in the nanoporous material. This model enables us to evaluate and rank adsorbents for adsorbed xenon propellant storage. The performance of each adsorbed storage system is judged by the mass of storage materials – composed of the walls of the pressure vessel and the mass of the adsorbent material – required to carry the

[a] *School of Chemical, Biological, and Environmental Engineering, Oregon State University, Corvallis, OR, USA. E-mail: Cory.Simon@oregonstate.edu*
[b] *Department of Physics, Oregon State University, Corvallis, OR, USA*
[c] *Pacific Northwest National Laboratory, Richland, WA, USA*

† Electronic supplementary information (ESI) available. See DOI: 10.1039/d1ma00167a

xenon propellant needed for the mission. We use our model to find the optimal storage pressure, tailored to each nanoporous material, that minimizes the mass of the storage materials needed. Conventional, bulk xenon storage serves as a baseline for evaluating porous materials for adsorbed xenon storage. Thus, we also use our model to find the minimal-mass pressure vessel under a bulk storage strategy. Our hypothesis is that the optimal storage pressure for an adsorbed xenon storage systems is lower than that of the bulk xenon storage system, thereby allowing for thinner-walled and thus lighter pressure vessels in the adsorbed storage system. The important question our model addresses is whether the reduced mass of the pressure vessel in the adsorbed xenon system compensates for the (additional) mass of the adsorbent required to store the xenon at a lower pressure. The answer to this question depends on the xenon adsorption isotherm in and density of the nanoporous material.

We use our model to assess several nanoporous materials for xenon propellant storage, using experimentally reported xenon adsorption isotherms as input. We find that MOF-505 and Ni-MOF-74 outperform the traditional adsorbent, activated carbon. However, when comparing the adsorbed and bulk xenon storage systems, we find that none of the nanoporous materials considered compete with the bulk storage system in terms of reducing the overall mass of the storage system. On the basis of a strong relationship between the adsorbent performance and its xenon adsorption properties, our model suggests the saturation loading of xenon in the adsorbent must exceed *ca.* 94 mmol Xe g^{-1} for the adsorbed storage system to be lighter than the bulk storage system. Also, nanoporous materials that exhibit high gravimetric surface areas tend to perform well for adsorbed xenon storage. Our conclusions rest on several simplifying assumptions, which we clearly list and discuss.

2 Modeling the pressure vessel, bulk xenon density, and xenon adsorption in the adsorbent

In this section, we formulate the mathematical models we use to describe the pressure vessel, bulk xenon gas, and xenon adsorption in the adsorbent. We later couple these models together to compose our models of both a bulk and adsorbed xenon propellant storage system. Table 1 summarizes the parameters and variables in our model.

2.1 The pressure vessel: spherical and thin-walled

Take the pressure vessel storing the xenon, in either the bulk or adsorbed phase, as a spherical shell composed of a homogeneous, elastic material. Let r [m] be the inner radius of the shell and t [m] be the (uniform) thickness of the vessel walls. Here, we relate the pressure P [bar] of (bulk or adsorbed) xenon inside the vessel to the resulting circumferential stress σ [bar] internal to the material composing the vessel walls. We use this relation to set the thickness of the walls of the vessel to safely contain the xenon without rupturing.

By invoking the thin wall approximation,[21] assuming $r \gg t$, (i) the circumferential stress σ is spatially uniform in the material and (ii) we do not distinguish between the inner and outer radius r. A free body diagram on a hemisphere of the vessel (see Fig. 1) balances two opposing forces in the direction normal to the plane on which the hemisphere sits, arising from: (a) the circumferential stress in the material and (b) the pressure of the gas on the inner walls, giving:

$$P\pi r^2 = \sigma 2\pi r t. \tag{1}$$

We design the vessel by choosing the wall thickness t such that the wall stress σ is equal to $\beta\sigma_y$ where $\beta < 1$ is a safety factor and σ_y [bar] is the yield strength of the material composing the vessel walls:

$$t = \frac{Pr}{2\beta\sigma_y}. \tag{2}$$

We assume the vessel walls are composed of a titanium alloy (Ti–6Al–4V) commonly used for aerospace applications[22,23] with yield strength σ_y = 8250.0 [bar][23] and density ρ_v = 4429 kg m^{-3}.[22] *N.B.* mechanical properties of alloys could depend on whether they are under uniaxial or biaxial stress.[24] We use a safety factor β = 0.5 as in ref. 25.

2.2 Density of bulk xenon fluid: interpolation of NIST data

We interpolate data from the NIST Chemistry WebBook[26] to characterize the density of bulk xenon gas, ρ_{Xe} [mol m^{-3}], as a function of pressure, P, at constant temperature, T = 298 K.

Table 1 Description of model parameters/variables

Symbol	Description	Units
n_{Xe}	Moles of xenon required for mission	mol
P	Pressure of xenon gas in the bulk- or adsorbed-storage vessel	bar
ρ_{Xe}	Density of xenon gas in the bulk phase	mol m^{-3}
ρ_{Xe}^{ads}	Density of xenon gas in the adsorbent (absolute adsorption)	mol m^{-3}
K	Langmuir parameter: describes xenon-adsorbent affinity	bar^{-1}
M	Langmuir parameter: saturation loading of xenon in the adsorbent	mol kg^{-1}
ρ_{ads}	Bulk density of the (empty) adsorbent	kg m^{-3}
ρ_v	Density of the material composing the vessel walls	kg m^{-3}
σ_y	Yield strength of material composing the vessel walls	bar
m_v	Mass of material composing the vessel walls	kg
m_{ads}	Mass of adsorbent filling the vessel	kg
w_{Xe}	Molar mass of xenon	kg mol^{-1}

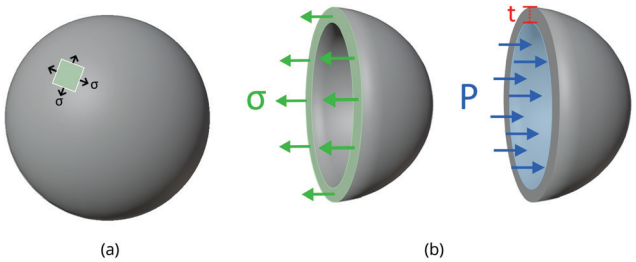

Fig. 1 Thin-walled, spherical pressure vessel model. (a) A spherical pressure vessel (a shell of homogeneous material). A patch is shown on an arbitrary location, subject to biaxial stress σ. The stress σ is internal to the material comprising the walls of the vessel and, under the thin-wall approximation, is spatially uniform within the material. (b) A static free-body diagram of half of the spherical pressure vessel, showing the circumferential stress σ inside the walls, giving rise to a force that balances the force arising from the pressure P exerted on the plane by the xenon fluid inside. The thickness of the wall of the vessel is t.

Fig. 2 displays $\rho_{Xe} = \rho_{Xe}(P;T)$. Note that 298 K is above the critical temperature of xenon (T_c = 289.74 K). Near the critical pressure of xenon (P_c = 58.42 bar), small changes in pressure result in large changes in density.

For comparison, we also show the density of the ideal gas in Fig. 2. The ideal gas law is not sufficiently accurate for describing the density of xenon at high pressures relevant to propellant storage. As a result of attractions between the xenon particles, the xenon fluid exhibits a higher density than the ideal gas in the pressure range shown in Fig. 2.

2.3 Density of adsorbed xenon: the Langmuir adsorption model

To describe the density of adsorbed xenon in a porous material, ρ_{Xe}^{ads} [mol m^{-3}], as a function of pressure and at fixed temperature, we use Langmuir's single-site equilibrium adsorption model:[27]

$$\rho_{Xe}^{ads}(P) = \rho_{ads} M \frac{KP}{1+KP}, \quad (3)$$

where M [mol kg^{-1}] is the saturation loading of xenon in the adsorbent, K [bar^{-1}] is the Langmuir parameter, the inverse of the pressure at which half the adsorption sites are occupied and a metric of the affinity of xenon for the material, and ρ_{ads} [kg m^{-3}] is the bulk density of the adsorbent (when devoid of gas); this makes $M\rho_{ads}$ [mol m^{-3}] the density of adsorption sites in the adsorbent.

For the purposes of modeling adsorbed xenon storage, under the single-site Langmuir model, a porous material is fully characterized by M, K and ρ_{ads}. Volumetric (ρ_{Xe}^{ads}) and gravimetric ($\rho_{Xe}^{ads}/\rho_{ads}$) xenon adsorption in the material, both of which are important for xenon propellant storage, are related by ρ_{ads}.

For each adsorbent material under consideration:

- We identify its Langmuir model parameters K and M from its experimentally measured, gravimetric xenon adsorption isotherm [mol Xe kg^{-1} adsorbent] in a least-squares fitting routine. As opposed to constructing $\rho_{Xe}^{ads}(P)$ by interpolating the data, the Langmuir model allows us to extrapolate the adsorbed density to larger pressures than observed in the experiments (*ca.* 0–1 bar).
- We approximate the bulk density ρ_{ads} of each nanoporous material as equal to its crystal density. We revisit this assumption later for materials with reported bulk densities.[28] The bulk density depends on the form of the material (powder, pellet, *etc.*)[29–31] but is typically less than the crystal density owing to interstitial voids.[28]

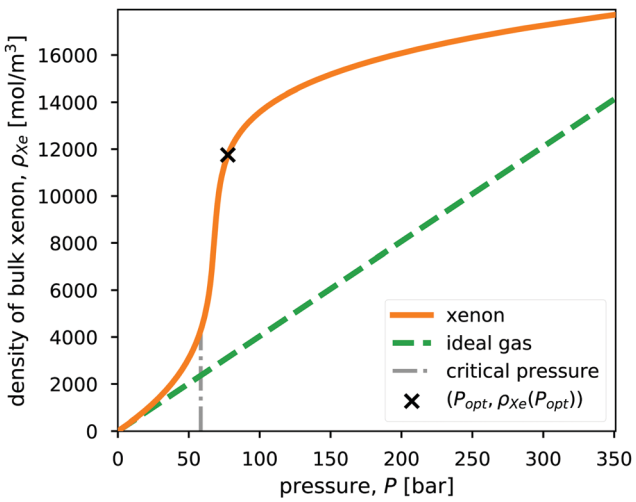

Fig. 2 The density of xenon, $\rho_{Xe} = \rho_{Xe}(P)$, as a function of pressure, P, at a fixed temperature of 298 K, taken from NIST.[26] For comparison, the density of the ideal gas is also shown. The vertical, dashed line marks the critical pressure of xenon (P_c = 58.42 bar. Note T_c = 289.74 K.). The x marks the optimal storage conditions in a bulk xenon propellant storage system, which we will derive later.

3 Xenon storage

We now couple the models for the xenon fluid, pressure vessel, and adsorbent to formulate a model for both bulk- and adsorbed-xenon storage systems. For both storage strategies, our first goal is to determine the mass of storage materials– the mass of material composing the walls of the pressure vessel and, if adsorbed-xenon storage, the mass of the adsorbent material– needed to carry the n_{Xe} [mol] of xenon required for the mission. The mass of storage materials required is a function of our choice of storage pressure. Our second goal is to then find the storage pressure, for both bulk- and adsorbed-xenon propellant storage systems, that minimizes the mass of storage materials. The primary performance metric of a given xenon propellant storage system is the tankage fraction: the mass of storage materials required per mass of xenon propellant stored.[25]

3.1 Bulk xenon propellant storage

In bulk xenon storage, we compress the pure xenon fluid and contain it in a free-space, spherical pressure vessel.

The volume of the vessel required‡ to store the n_{Xe} [mol] of xenon is n_{Xe}/ρ_{Xe}. Thus, the radius of the spherical vessel as a

‡ Recall, under the thin-walled vessel approximation, we do not distinguish between an outer- and inner-volume.

function of storage pressure is:

$$r = r(P) = \left(\frac{3}{4\pi}\frac{n_{Xe}}{\rho_{Xe}(P)}\right)^{1/3}. \quad (4)$$

Substituting $r(P)$ into the stress model for the vessel in eqn (2), we arrive at the required thickness of the vessel, $t = t(P)$, to safely contain the compressed xenon. Finally, the mass of material comprising the walls of the pressure vessel is, after (conceptually) flattening the vessel walls:

$$m_v = 4\pi r^2 t\rho_v = m_v(P) = \frac{3n_{Xe}\rho_v P}{2\beta\sigma_y\rho_{Xe}(P)}, \quad (5)$$

where ρ_v is the density of the material composing the vessel walls. Intuitively, m_v scales with the density of the material composing the walls of the vessel, ρ_v, and with the required amount of xenon for the mission, n_{Xe}. On the other hand, m_v scales inversely with the yield stress of the vessel material, σ_y.

3.1.1 Optimizing the storage pressure. The optimal storage pressure P_{opt} [bar] minimizes the material composing the vessel walls that is required to safely contain the n_{Xe} [mol] xenon for the mission:

$$P_{opt} = \arg\min_P [m_v(P)]. \quad (6)$$

We minimize $m_v(P)$ numerically to find P_{opt}. The associated tankage fraction of the optimized bulk-storage vessel is then:

$$\mathcal{T}_{opt} := \frac{m_v(P_{opt})}{n_{Xe}w_{Xe}}, \quad (7)$$

with w_{Xe} the molar mass of xenon.

3.2 Adsorbed xenon propellant storage

In adsorbed xenon storage, we fully pack the spherical pressure vessel with porous material to store xenon gas in the adsorbed phase.

The mass of adsorbent m_{ads} needed for the mission, as a function of storage pressure, P, is

$$m_{ads} = m_{ads}(P) = \frac{\rho_{ads}n_{Xe}}{\rho_{Xe}^{ads}(P)}, \quad (8)$$

with the density of adsorbed xenon, ρ_{Xe}^{ads}, given by the Langmuir adsorption model in eqn (3). Imposing the volume of the vessel to be equal to the volume of the adsorbent required, the radius of the spherical pressure vessel is:

$$r = r(P) = \left(\frac{3}{4\pi}\frac{n_{Xe}}{\rho_{Xe}^{ads}(P)}\right)^{1/3}, \quad (9)$$

which is eqn (4) with the bulk xenon density replaced with the adsorbed xenon density.

The required thickness of the vessel walls, $t = t(P)$, follows from substituting $r(P)$ into the stress model for the vessel in eqn (2). Finally, the mass of material composing the walls of the pressure vessel is:

$$m_v = 4\pi r^2 t\rho_v = m_v(P) = \frac{3n_{Xe}\rho_v P}{2\beta\sigma_y\rho_{Xe}^{ads}(P)}, \quad (10)$$

which is eqn (5) with the bulk xenon density replaced with the adsorbed xenon density.

3.2.1 Optimizing the storage pressure. The storage pressure that minimizes the total mass of storage materials required to carry the xenon for the mission is found analytically (setting the derivative equal to zero):

$$P_{opt} := \arg\min_P [m_{ads}(P) + m_v(P)] = \sqrt{\frac{2\beta\sigma_y\rho_{ads}}{3K\rho_v}}. \quad (11)$$

This optimum storage pressure balances the mass of the adsorbent required, which decreases with increasing pressure, and the mass of the vessel walls required to contain the pressure. Intuitively, the optimal storage pressure is low when using porous materials that adsorb xenon strongly (large K) and high if the porous material is very dense (large ρ_{ads}) or if the vessel walls have a high yield strength (large σ_y).

Finally, the minimal mass of storage materials required for the mission is $m_{ads}(P_{opt}) + m_v(P_{opt})$. The optimal tankage fraction is then:

$$\mathcal{T}_{opt} := \frac{m_{ads}(P_{opt}) + m_v(P_{opt})}{n_{Xe}w_{Xe}} = \frac{1}{M\rho_{ads}w_{Xe}}\left(\sqrt{\rho_{ads}} + \sqrt{\frac{3\rho_v}{2\sigma_y\beta K}}\right)^2. \quad (12)$$

The effects of material properties on the tankage fraction are apparent: to provide a small tankage fraction, we wish for:

- the material composing the vessel walls to be light (small ρ_v) and strong (large σ_y).
- the adsorbent material to be light (small ρ_{ads}), strongly adsorb xenon (large K), and have a large number of xenon adsorption sites packed per volume (large $M\rho_{ads}$).

While these effects of material parameters on the tankage fraction are qualitatively unsurprising, eqn (12) allows us to quantitatively evaluate several adsorbents for adsorbed xenon propellant storage and compare to the bulk storage strategy.

3.3 Remarks

Conveniently, the optimal storage pressure and tankage fraction do not depend on the amount of xenon required for the mission, n_{Xe}, for both bulk and adsorbed storage systems (see eqn (5) and (7) and eqn (11) and (12), respectively). However, the choice of the safety factor β could affect (i) the ranking of adsorbents according to their optimal tankage fractions (see eqn (12)) and (ii) the ratio of the bulk to adsorbed optimal tankage fractions (divide eqn (7) by eqn (12)).

While eqn (12) shows the effects of material parameters on the optimal tankage fraction, these material parameters are intimately coupled and correlated, and therefore generally cannot be independently tuned. *E.g.*, denser materials tend to more strongly attract xenon, giving rise to a positive correlation between ρ_{ads} and K.

4 Results

We now evaluate several porous materials for adsorbed xenon propellant storage, with bulk xenon storage as a baseline. The data and Julia code to fully reproduce our calculations and plots are available at github.com/SimonEnsemble/PropellantStorage.

Without loss of generalization, we take the required mass of propellant needed for the mission as $n_{Xe}w_{Xe}$ = 100 kg.

4.1 Compressed, bulk xenon storage

As a baseline, we first analyze a bulk xenon storage system, where xenon gas is compressed and stored in a spherical, thin-walled pressure vessel, without an adsorbent.

Fig. 3 shows the radius, wall thickness, and tankage fraction for bulk xenon storage over a pressure range of 20 bar to 125 bar. The optimal storage pressure is P_{opt} = 77.6 bar, which provides a minimal tankage fraction of $\mathcal{T}_{opt}$ = 0.08. Notably, $P_{opt} > P_c$ to exploit the large slope of $\rho_{Xe}(P)$ in Fig. 2, where a small change in pressure results in a large change in xenon density. See the x in Fig. 2 that marks $(P_{opt},\rho_{Xe}(P_{opt}))$.

4.2 Adsorbed xenon storage

Next, we evaluate and compare the performance of several porous materials for adsorbed xenon propellant storage, with the bulk storage system as a baseline.

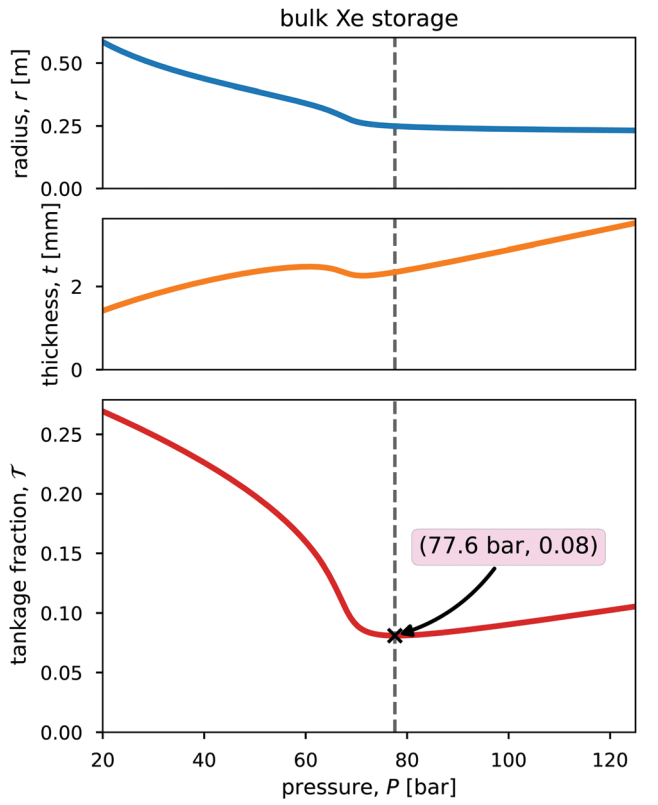

Fig. 3 Optimizing the compressed, bulk xenon storage system at 298 K. The radius of the vessel, the thickness of its walls, and the tankage fraction are shown as a function of the storage pressure. The optimal storage pressure (vertical, dashed line) minimizes the tankage fraction.

4.2.1 The porous material candidates. As candidate nanoporous material adsorbents for adsorbed xenon propellant storage, we consider the MOFs, SBMOF-1,[32] Ni-MOF-74,[33] HKUST-1,[34] SBMOF-2,[35] $Co_3(HCOO)_6$,[36] MOF-505[37] (= NOTT-100[38]), and $Ni(PyC)_2$[39] and POC material CC3.[40] We also consider activated carbon as a baseline. We selected these materials because their experimentally measured xenon adsorption isotherms near 298 K are available in the literature.[17,35,39,41–44] Fig. 3 displays the crystal structures of the candidate nanoporous materials and their crystal densities (= ρ_{ads}). For activated carbon, which is amorphous, we took the density as that of 1230C coconut shell activated carbon, used in ref. 44, from the data sheet in ref. 45, 500 kg m^{-3}.

4.2.2 The adsorbed xenon density in each porous material. We use the Langmuir adsorption model $\rho_{Xe}^{ads}(P)$ in eqn (3) to describe the adsorbed density of xenon in each material as a function of pressure. We identify the Langmuir parameters M and K for each adsorbent by fitting $\rho_{Xe}^{ads}(P)/\rho_{ads}$ to the experimentally measured, gravimetric (per mass of adsorbent) xenon adsorption data at 298 K (with the exception of MOF-505, 292 K and Ni-MOF-74, 297 K). Fig. S1 (ESI†) shows the raw gravimetric xenon adsorption data and the gravimetric Langmuir model fits, all of which reasonably describe the shape formed by the data. Table 2 lists the identified Langmuir parameters M and K for each adsorbent, in addition to the references for the adsorption data. Finally, Fig. 5a displays (i) the volumetric (per volume of adsorbent) xenon adsorption data, converted from the gravimetric adsorption data using ρ_{ads}, (ii) the fitted models for the adsorbed xenon density, $\rho_{Xe}^{ads}(P)$, and (iii) the bulk gas density $\rho_{Xe}(P)$. The plot shows a larger pressure range than Fig. S1 (ESI†), on a logarithmic scale, to see how the model $\rho_{Xe}^{ads}(P)$ extrapolates to pressures larger than found in the data. Compared with the bulk xenon density at the same temperature and pressure, adsorbents achieve a much higher xenon density at lower pressures (*ca.* $<$40 bar), but, at higher pressures, the bulk density is greater because the skeleton of the adsorbent occupies a fraction of the space and excludes xenon adsorbates.

Although xenon adsorption data was also available for IRMOF-1[46] and PCN-12,[42] we omit these MOFs from our analysis because their xenon adsorption isotherms do not exhibit a plateau, preventing reliable estimation of M to extrapolate the adsorbed xenon density beyond the maximum pressure observed in the data, *ca.* 1 bar.

To summarize the properties of the adsorbents that dictate their performance for adsorbed xenon propellant storage, Fig. 5b displays the distributions and correlations between the adsorbent parameters K, M, and ρ_{ads}.

4.2.3 Optimizing the adsorbed-xenon storage system for each material. For each adsorbent, we find the optimal storage pressure, P_{opt} in eqn (11), and the associated optimal tankage fraction, given in eqn (12). Fig. 6a summarizes the performance of the materials for adsorbed xenon propellant storage, with the aim of minimizing the mass of storage materials required to carry the xenon propellant into space. The x's in Fig. 5a mark $(P_{opt},\rho_{Xe}^{ads}(P_{opt}))$ for each adsorbent.

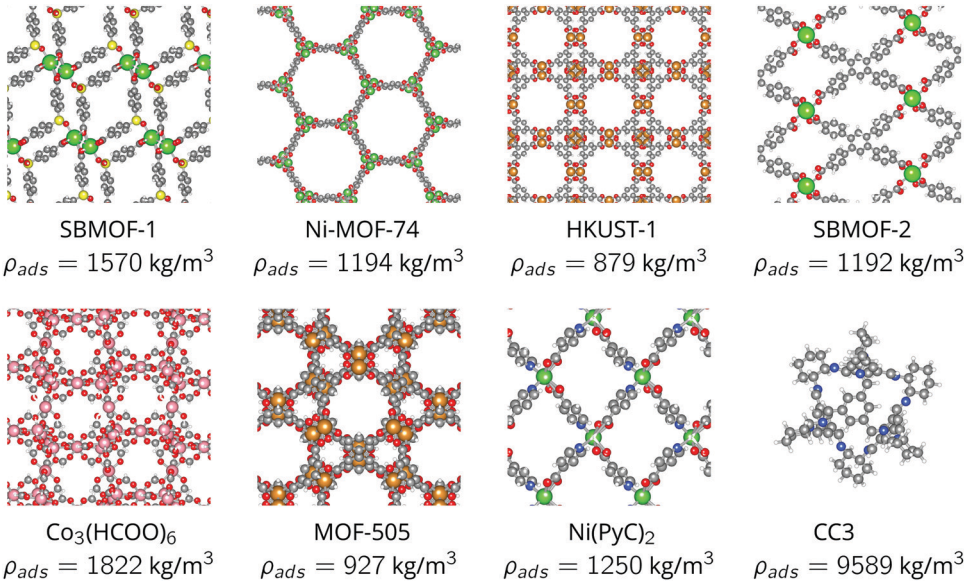

Fig. 4 The crystal structures of the nanoporous material candidates we consider for adsorbed xenon propellant storage and their (crystal) densities, ρ_{ads}. For CC3, a molecular material, we show only a single cage.

Table 2 The identified Langmuir model parameters in the candidate materials

Material	M [mol kg^{-1}]	K [bar^{-1}]	Reference for adsorption data
MOF-505	12.37	0.98	42
Ni-MOF-74	7.17	1.52	17
Activated-Carbon	5.26	2.26	44
SBMOF-2	3.71	3.27	35
Ni(PyC)$_2$	3.30	18.9	39
HKUST-1	2.99	2.04	17
CC3	2.74	7.57	43
$Co_3(HCOO)_6$	2.30	6.50	41
SBMOF-1	1.41	37.2	17

Ranking the adsorbents. The adsorbents in Fig. 6b are ranked by the optimal tankage fraction. Ni-MOF-74 and MOF-505 provide lower tankage fractions than an adsorbed xenon storage system based on the traditional adsorbent, activated carbon.

Bulk vs. adsorbed xenon storage. The optimal storage pressures for the adsorbed xenon storage systems are lower than for the bulk storage system; however, the optimal tankage fractions of the adsorbed storage systems are larger. Fig. 6b shows, with the bulk storage system as a baseline, the adsorbents reduce the mass of the vessel walls required to store the xenon, but at the expense of (i) achieving a lower density of xenon, resulting in a larger pressure vessel and (ii) carrying a large mass of adsorbent material. In conclusion, according to our mathematical model, the adsorbents provide a reduction (compared to bulk storage) in the mass of the vessel walls, owing to reduced storage pressures, but this does *not* compensate for the (additional) mass of the adsorbent material itself; for each adsorbent, the mass of the storage materials (vessel walls + adsorbent) required to carry the xenon into space is greater than the mass of the storage materials (vessel walls) for the bulk storage system.

4.2.4 Relationship between performance and adsorption properties. What properties of an adsorbent are desirable for xenon propellant storage? Addressing this question could lead to improved adsorbents that yield an adsorbed xenon storage system with a lower tankage fraction than bulk storage. While eqn (12) provides insights into how K, M, and ρ_{ads} influence the optimal tankage fraction, these parameters are in practice not independent, but correlated (see Fig. 5b).

The saturation loading, M, of the adsorbent is a strong predictor of the optimal tankage fraction of the adsorbed xenon storage system. See Fig. 7. Eqn (12) provides an explanation, by noting the tendency for (i) the mass of the adsorbent to dominate the optimal tankage fraction (see Fig. 6b) and (ii) $KP_{opt} \gg 1$, giving the approximation to the optimal tankage fraction:

$$\frac{m_{ads}(P_{opt}) + m_v(P_{opt})}{n_{Xe} w_{Xe}} \approx \frac{m_{ads}(P_{opt})}{n_{Xe} w_{Xe}} = \frac{1}{M w_{Xe}}\left(1 + \frac{1}{KP_{opt}}\right) \approx \frac{1}{M w_{Xe}}. \quad (13)$$

This approximation is shown as the curve in Fig. 7, along which the data approximately lie. So, the performance of an adsorbent for adsorbed xenon propellant storage tends to be determined by, to first order, its saturation loading, M. This result is intuitive because (i) the optimal storage pressure tends to be near saturation conditions ($KP_{opt} \gg 1$), (ii) we wish to minimize the mass of storage materials, dominated by the adsorbent, and (iii) M is the amount of Xe stored per mass of adsorbent at saturation conditions.

We use the approximation in eqn (13) to estimate that, for an adsorbed storage system to give a lower optimal tankage fraction than the bulk storage system, the saturation loading of xenon in the adsorbent must exceed 94 mol kg^{-1}, much larger

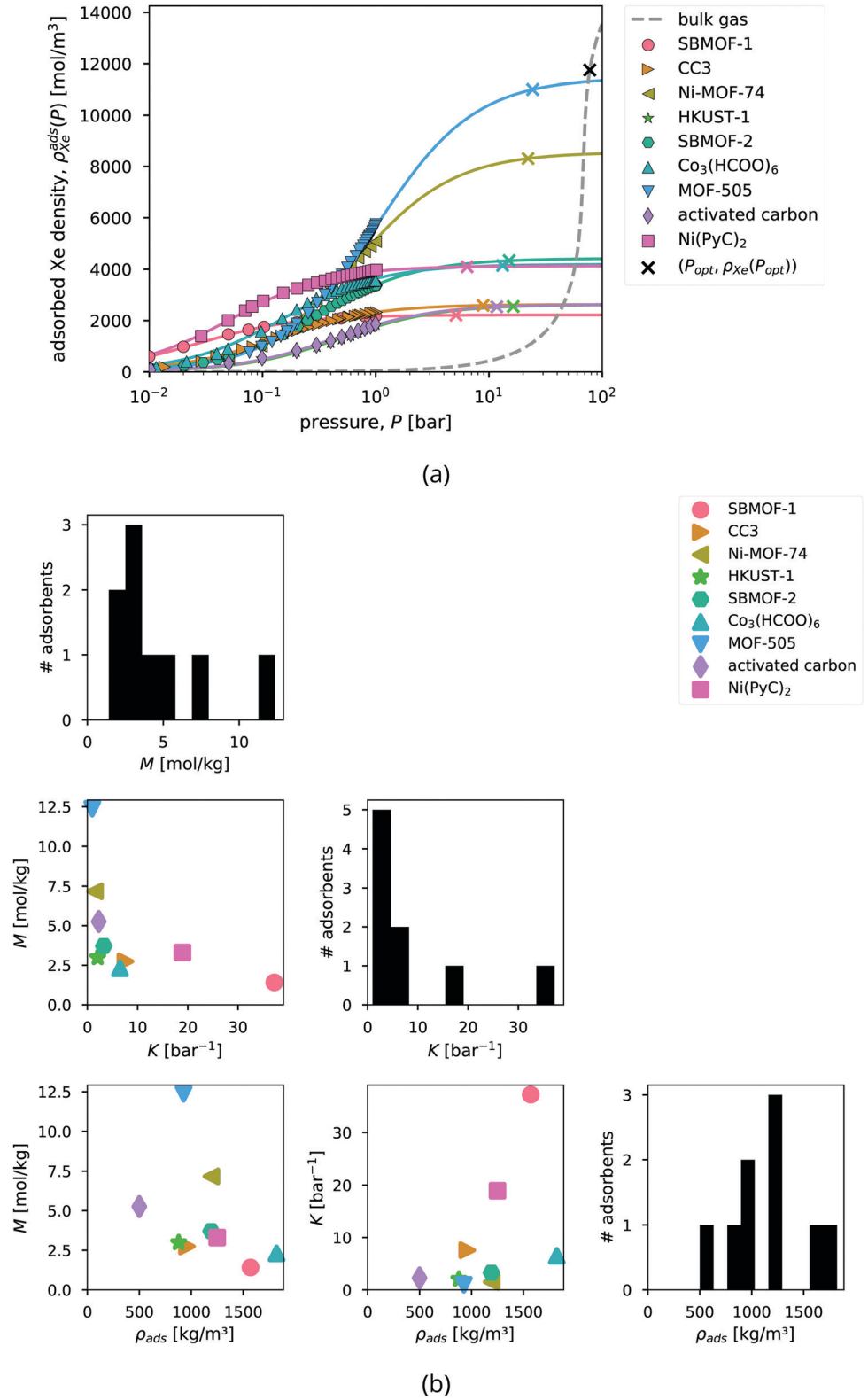

Fig. 5 Xenon adsorption in the candidate adsorbents. (a) Curves show the fitted Langmuir adsorption model, $\rho_{Xe}^{ads}(P)$ in eqn (3), to describe the adsorbed xenon density in each adsorbent at 298 K. Points show the experimentally measured xenon adsorption isotherms (at 298 K, except for MOF-505, 292 K, and Ni-MOF-74, 297 K), converted from the raw gravimetric adsorption data using ρ_{ads}. The dashed curve shows the density of the bulk gas, $\rho_{Xe}(P)$. The x's mark the optimal storage conditions (P_{opt},$\rho_{Xe}^{ads}(P_{opt})$) that we will derive later. (b) The distributions (diagonal) and correlations between (off-diagonal) the Langmuir M, Langmuir K, and density ρ_{ads} of the adsorbents.

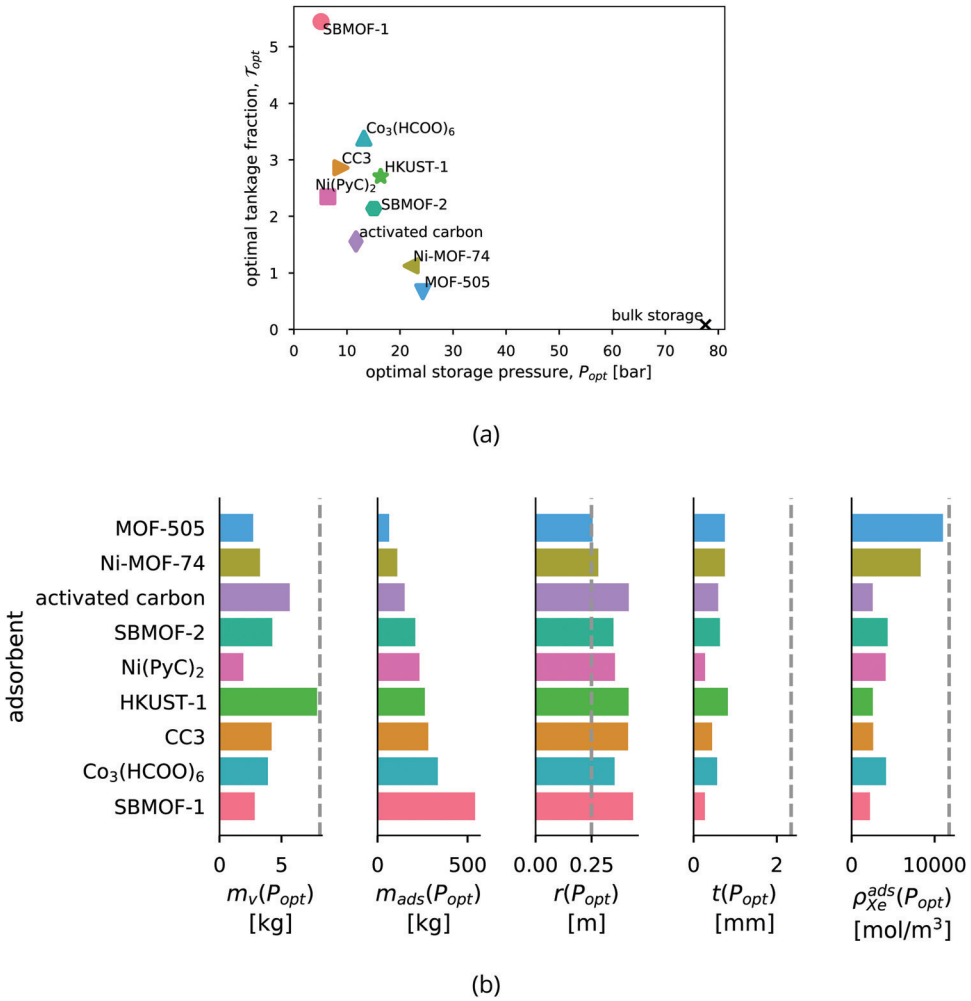

Fig. 6 Performance of the optimized adsorbed xenon propellant storage systems. (a) The optimal storage pressure P_{opt} and associated optimum tankage fraction for each adsorbent. As a baseline, the bulk storage system is depicted by the *x*. (b) For each optimized adsorbed Xe storage system: the mass of the pressure vessel walls, mass of adsorbent material, radius of the vessel, thickness of the vessel walls, and density of adsorbed xenon. Where relevant, the horizontal dashed lines show the corresponding characteristic for the optimized bulk storage system.

than seen for the adsorbents in Table 2. Based on the relationship between M and ρ_{ads} in Fig. 5b, such an adsorbent must not be dense. Indeed, lighter adsorbents (lower ρ_{ads}) also tend to give adsorbed Xe storage systems with lower optimal tankage fractions; see Fig. S2 (ESI†).

We also find that nanoporous materials that exhibit high gravimetric surface areas (defined by the zero potential energy contour of a xenon adsorbate in the pores, computed in iRASPA[47,48]) tend to provide lower tankage fractions. See Fig. S3 (ESI†). Similarly, virtual screenings of MOFs for hydrogen storage show that MOFs with high gravimetric surface areas tend to have the highest deliverable capacities of hydrogen;[49] however, for methane storage, intermediate gravimetric surface areas are desirable.[50]

5 Limitations

Our mathematical model and the conclusions we extract from it are subject to several limitations emanating from simplifying model assumptions. We discuss some of these below.

The safety factor

The choice of the safety factor influences the comparison between adsorbents and between adsorbed and bulk storage systems (see eqn (5) and (12)) because it scales the contribution to the tankage fraction by the metal composing the vessel walls. We crudely investigated the sensitivity of our results to β: only when $\beta < \approx 0.05$ does the tankage fraction of MOF-505 compete with the bulk storage system. For this very low β, only CC3 and HKUST-1 switch rankings, indicating the ranking of adsorbents here is insensitive to the choice of β.

Extrapolation of data on adsorbed xenon density in the nanoporous materials

We used fitted Langmuir adsorption models to extrapolate experimental adsorption data, which is available only up to *ca.* 1 bar (see Fig. 5a). Though we excluded adsorbents from our study whose adsorption isotherm data did not exhibit a plateau for reliable estimation of the saturation loading M, this extrapolation could still introduce significant error.

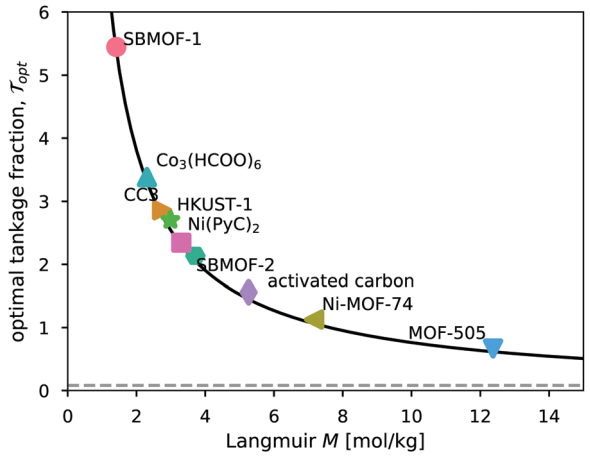

Fig. 7 The relationship between the tankage fraction of each optimized adsorbed xenon storage system and the saturation loading of xenon in the adsorbent, M. The solid curve shows the approximation to the optimal tankage fraction in eqn (13).

Bulk *vs.* crystal density of the nanoporous materials

The bulk density of the nanoporous material, ρ_{ads}, influences the optimum storage pressure and tankage fraction of the adsorbed xenon storage system. See eqn (11) and (12). For each nanoporous material, we approximated ρ_{ads} as its crystal density (easily computed from its crystal structure, listed in Fig. 4) because bulk densities were not reported for each nanoporous material in our study. However, in practice, the adsorbent when packed into a pressure vessel will take the form of a compacted powder forming granules or pellets; the bulk density of such MOF powders is usually lower than the crystal density owing to interstitial voids.[28–31,51]

We now investigate how our approximation, bulk density of the nanoporous material $\rho_{ads} \approx$ crystal density, influences our results. We properly used measured bulk/tap densities reported for CC3, HKUST-1, and Ni-MOF-74[28] (see Fig. S4a, ESI†) for ρ_{ads} in our model to investigate how the tankage fraction changes for these materials, compared to when we used the crystal density. Fig. S4b (ESI†) shows that, for these three materials for which the bulk density was available: when inputting into our model the more realistic bulk density for ρ_{ads} instead of the crystal density, the optimal storage pressures are reduced, but, the tankage fraction increases only marginally. The latter is consistent with the approximation of the tankage fraction in eqn (13), which does not involve ρ_{ads}. *I.e.*, the approximation bulk density $\approx$ crystal density is unlikely to influence our conclusion that the adsorbed storage systems we considered do not provide lower tankage fractions than a bulk storage system.

The paucity of material space sampled

We only considered the eight nanoporous materials in Fig. 4 owing to a paucity of experimentally measured xenon adsorption isotherms for input to our model. Fig. 5b displays the diversity of the material parameters $\{M,K,\rho_{ads}\}$ among this set of materials. There are thousands of additional existing MOFs[52,53] that could, possibly, provide a lower tankage fraction than the bulk storage system.

Thin-wall approximation for the pressure vessel

We invoked the thin-wall approximation to determine the thickness of the walls of the pressure vessel *via* eqn (2). Fig. 3 and 6b show that, indeed, $r \gg t$, making this approximation reasonable.

Geometry of the pressure vessel

We took the pressure vessel to be a sphere. Different pressure vessel geometries will require a different mechanical model to determine the mass of vessel material needed to safely contain the xenon.

A pressure vessel composed of a titanium alloy

For a simple estimate, we took the pressure vessel as composed of a titanium alloy. In practice, composite overwrapped pressure vessels (COPVs) are typically used for xenon propellant storage. In a COPV, a gas-impermeable, metallic inner-liner is overwrapped with a strong, permeable carbon fiber overwrap such as Kevlar. The partnership between these materials could allow for a lighter pressure vessel.[54,55]

Residual gas in the adsorbent

A consideration for adsorbed gas storage is the residual gas trapped in the adsorbent at the desorption conditions. Studies on vehicular methane or hydrogen gas storage and delivery *via* adsorbents use the *deliverable capacity* of the gas in the material- the density of gas in the material at the storage condition minus the residual gas at the discharge condition[56,57]- as a performance metric for the material. We assumed the deliverable capacity of xenon in the adsorbent is equal to the adsorbed xenon density at the storage pressure because, in space, the discharge pressure corresponds to vacuum. *I.e.*, we assume that the xenon gas adsorbed in the material at the storage pressure P can be fully delivered.

Temperature of 298 K

We assumed a constant storage temperature of 298 K, as in ref. 8 and 25. The performance of adsorbents compared to bulk storage could be improved by lowering the storage temperature, since generally adsorbents will achieve a higher adsorbed xenon density at lower temperatures. However, the insulation and/or refrigeration system required to maintain a lower storage temperature[25] would contribute more mass to the storage system and complicate its design.

6 Conclusions and future work

We formulated a simple mathematical model of an adsorbed xenon propellant storage system by coupling (i) a stress model for the thin-walled, spherical pressure vessel and (ii) a Langmuir adsorption model to describe the adsorbed xenon density in the porous material. We used the model to find the optimum

storage pressure that minimizes the mass of the storage materials (composed of (i) the metal comprising the walls of the pressure vessel and (ii) the adsorbent material) required to carry the xenon onboard the spacecraft. We derived eqn (11) and (12), interpretable expressions for the optimum storage pressure and associated minimum tankage fraction, revealing how properties of the materials (both the metal and the adsorbent) affect the performance of the adsorbed xenon storage system. Fig. 6 compares the performance of several adsorbent materials for Xe propellant storage, with bulk Xe storage as a baseline.

We conclude that, for the adsorbent materials considered in Fig. 4, the reduction in the mass of the pressure vessel walls, enabled by reduced storage pressures provided by the adsorbents, does not compensate for the added mass of adsorbent material. That is, an adsorbed Xe storage system does not provide weight savings compared to the bulk Xe storage system. Because the mass of the adsorbent dominates the tankage fraction, the tankage fraction is, to first order approximation, inversely related to the gravimetric saturation loading of xenon in the adsorbent [units: amount of Xe per mass of adsobent]. Our model suggests to, in pursuit of an adsorbent that can outperform the bulk storage system, search for adsorbents that (i) are not dense and (ii) have a very high gravimetric xenon saturation loading, >94 mmol Xe g^{-1} adsorbent.

Ni-MOF-74 and MOF-505 do, however, offer an improved tankage fraction over the traditional adsorbent, activated carbon, which was previously considered for xenon propellant storage.[10]

N.B., the optimal storage pressure and tankage fraction of an adsorbed Xe propellant storage system depend on the xenon adsorption isotherm in the adsorbent, the density of the adsorbent, and the properties (density, yield strength) of the material composing the walls of the pressure vessel.

Our model is only a first-order approximation/Fermi estimate to approach the question of whether nanoporous materials are a worthy pursuit for xenon propellant storage, with the objective of minimizing the mass of the storage materials. We listed and discussed several limitations of our model above.

Future work includes (a) developing a COPV stress model and coupling it with the adsorbent model, (b) considering different tank geometries, and (c) expanding the scope of adsorbent materials considered by *e.g.*, a high-throughout computational screening of materials for xenon propellant storage.[58–60]

Conflicts of interest

There are no conflicts of interest to declare.

Acknowledgements

N. G., P. K. T., and C. M. S. acknowledge the U.S. Department of Defense (DoD) Defense Threat Reduction Agency (HDTRA-19-31270) for the necessary funding and support. PNNL is operated by Battelle for the U.S. DOE under contract DE-AC05-76RL01830. We thank our DTRA program manager Dr Calvin L. Shipbaugh for support. M. T. H. and S. H. thank the Pete and Rosalie Johnson Internship Program at Oregon State University.

References

1 J. S. Sovey, V. K. Rawlin and M. J. Patterson, Ion propulsion development projects in US: Space Electric Rocket Test I to Deep Space 1, *J. Propul. Power*, 2001, **17**(3), 517–526.
2 J. R. Brophy, NASA's Deep Space 1 ion engine (plenary), *Rev. Sci. Instrum.*, 2002, **73**(2), 1071–1078.
3 V. Rawlin, M. Patterson and R. Gruber, Xenon ion propulsion for orbit transfer, in *21st International Electric Propulsion Conference*, page 2527, 1990.
4 J. R. Beattie, J. N. Matossian and R. Robson, Status of xenon ion propulsion technology, *J. Propul. Power*, 1990, **6**(2), 145–150.
5 W. Tam, A. Jackson, E. Nishida, Y. Kasai, A. Tsujihata and K. Kajiwara, Design and manufacture of the ets viii xenon tank, in *36th American Institute of Aeronautics and Astronautics/American Society of Mechanical Engineers/Society of Automotive Engineers/American Society for Engineering Education Joint Propulsion Conference & Exhibit*, page 3677, 2000.
6 J. R. Beattie, J. N. Matossian, R. L. Poeschel, W. P. Rogers and R. M. Martinelli, Xenon ion propulsion subsystem, *J. Propul. Power*, 1989, **5**(4), 438–444.
7 J. Brophy, M. Marcucci, J. Gates, C. Garner, B. Nakazono and G. Ganapathi, Status of the DAWN ion propulsion system, in *40th AIAA/ASME/SAE/ASEE Joint Propulsion Conference and Exhibit*, page 3433, 2004.
8 J. R. Brophy, R. Y. Kakuda, J. E. Polk, J. R. Anderson, M. G. Marcucci, D. Brinza, M. D. Henry, K. K. Fujii, K. R. Mantha, J. F. Stocky, J. Sovey, M. Patterson, V. Rawlin, J. Hamley, T. Bond, J. Christensen, H. Cardwell, G. Benson, J. Gallagher, M. Matranga and D. Bushway, *Ion propulsion system (NSTAR) DS1 technology validation report*, Deep Space 1 Technology Validation Report-Ion Propulsion System (NSTAR), 2000.
9 B. Dunbar, Advanced space transportation program fact sheet, *National Aeronautics and Space Administration - Marshall Space Flight Center Archives*, 12, 2008.
10 D. D. Back, C. Ramos and J. A. Meyer. *Low-pressure long-term xenon storage for electric propulsion*, NASA, 2001.
11 H. Furukawa, K. E. Cordova, M. O'Keeffe and O. M. Yaghi, The chemistry and applications of metal-organic frameworks, *Science*, 2013, **341**(6149), 1230444.
12 A. I. Cooper, Porous molecular solids and liquids, *ACS Cent. Sci.*, 2017, **3**(6), 544–553.
13 C. S. Diercks and O. M. Yaghi, The atom, the molecule, and the covalent organic framework, *Science*, 2017, **355**(6328), eaal1585.
14 O. K. Farha, I. Eryazici, N. Cheon Jeong, B. G. Hauser, C. E. Wilmer, A. A. Sarjeant, R. Q. Snurr, S. B. T. Nguyen, A. ''Ozg''ur Yazaydn and J. T. Hupp, Metal-organic framework materials with ultrahigh surface areas: is the sky the limit?, *J. Am. Chem. Soc.*, 2012, **134**(36), 15016–15021.

15 Y. Song, Q. Sun, B. Aguila and S. Ma, Opportunities of covalent organic frameworks for advanced applications, *Adv. Sci.*, 2019, **6**(2), 1801410.
16 A. Schoedel, Z. Ji and O. M. Yaghi, The role of metal-organic frameworks in a carbon-neutral energy cycle, *Nat. Energy*, 2016, **1**(4), 1–13.
17 D. Banerjee, C. M. Simon, A. M. Plonka, R. K. Motkuri, J. Liu, X. Chen, B. Smit, J. B. Parise, M. Haranczyk and P. K. Thallapally, Metal-organic framework with optimally selective xenon adsorption and separation, *Nat. Commun.*, 2016, **7**(1), 1–7.
18 D. Banerjee, C. M. Simon, S. K. Elsaidi, M. Haranczyk and P. K. Thallapally, Xenon gas separation and storage using metal-organic frameworks, *Chem*, 2018, **4**(3), 466–494.
19 D. Banerjee, A. J. Cairns, J. Liu, R. K. Motkuri, S. K. Nune, C. A. Fernandez, R. Krishna, D. M. Strachan and P. K. Thallapally, Potential of metal-organic frameworks for separation of xenon and krypton, *Acc. Chem. Res.*, 2015, **48**(2), 211–219.
20 S. K. Elsaidi, D. Ongari, M. H. Mohamed, W. Xu, R. Kishan Motkuri, M. Haranczyk and P. K. Thallapally, Metal organic frameworks for xenon storage applications, *ACS Mater. Lett.*, 2020, **2**(3), 233–238.
21 C. T. Herakovich. Thin-walled pressure vessels, *A Concise Introduction to Elastic Solids*, Springer, 2017, pp. 77–81.
22 G. Welsch, R. Boyer and E. W. Collings, *Materials properties handbook: titanium alloys*, American Society for Metals International, 1993.
23 M. Niinomi, Mechanical properties of biomedical titanium alloys, *Mater. Sci. Eng., A*, 1998, **243**(1–2), 231–236.
24 C. W. Bert, E. J. Mills and W. S. Hyler. Mechanical properties of aerospace structural alloys under biaxial-stress conditions. Technical Report TR-66-229, Battelle Memorial Institute - Columbus Laboratories, Air Force Materials Laboratory, Wright-Patterson AFB, Ohio, 1966.
25 R. P. Welle, Propellant storage considerations for electric propulsion, in *22nd International Electric Propulsion Conference*, pages 91–107, 1991.
26 M. O. McLinden, E. W. Lemmon and D. G. Friend, *Thermophysical Properties of Fluid Systems'' in NIST Chemistry WebBook, NIST Standard Reference Database Number 69*, ed. P. J. Linstrom and W.G. Mallard, National Institute of Standards and Technology, Gaithersburg MD, 20899, retrieved February 5, 2020, DOI: 10.18434/T4D303.
27 H. Swenson and N. P. Stadie, Langmuir's theory of adsorption: A centennial review, *Langmuir*, 2019, **35**(16), 5409–5426.
28 K. J. Korman, G. E. Decker, M. R. Dworzak, M. M. Deegan, A. M. Antonio, G. A. Taggart and E. D. Bloch., Using low-pressure methane adsorption isotherms for higher-throughput screening of methane storage materials, *ACS Appl. Mater. Interfaces*, 2020, **12**(36), 40318–40327.
29 B. Valizadeh, T. N. Nguyen and K. C. Stylianou., Shape engineering of metal-organic frameworks, *Polyhedron*, 2018, **145**, 1–15.
30 M. Kunowsky, F. Suárez-Garca and Á. Linares-Solano, Adsorbent density impact on gas storage capacities, *Microporous Mesoporous Mater.*, 2013, **173**, 47–52.
31 J. Dhainaut, C. Avci-Camur, J. Troyano, A. Legrand, J. Canivet, I. Imaz, D. Maspoch, H. Reinsch and D. Farrusseng, Systematic study of the impact of MOF densification into tablets on textural and mechanical properties, *CrystEngComm*, 2017, **19**(29), 4211–4218.
32 D. Banerjee, Z. Zhang, A. M. Plonka, J. Li and J. B. Parise., A calcium coordination framework having permanent porosity and high CO_2/N_2 selectivity, *Cryst. Growth Des.*, 2012, **12**(5), 2162–2165.
33 N. L. Rosi, J. Kim, M. Eddaoudi, B. Chen, M. O'Keeffe and O. M. Yaghi, Rod packings and metal-organic frameworks constructed from rod-shaped secondary building units, *J. Am. Chem. Soc.*, 2005, **127**(5), 1504–1518.
34 S. S.-Y. Chui, S. M.-F. Lo, J. P. H. Charmant, A. G. Orpen and I. D. Williams., A chemically functionalizable nanoporous material $[Cu_3(TMA)_2(H_2O)_3]_n$, *Science*, 1999, **283**(5405), 1148–1150.
35 X. Chen, A. M. Plonka, D. Banerjee, R. Krishna, H. T. Schaef, S. Ghose, P. K. Thallapally and J. B. Parise, Direct observation of Xe and Kr adsorption in a Xe-selective microporous metal-organic framework, *J. Am. Chem. Soc.*, 2015, **137**(22), 7007–7010.
36 K. Li, D. H. Olson, J. Y. Lee, W. Bi, K. Wu, T. Yuen, Q. Xu and J. Li, Multifunctional Microporous MOFs Exhibiting Gas/Hydrocarbon Adsorption Selectivity, Separation Capability and Three-Dimensional Magnetic Ordering, *Adv. Funct. Mater.*, 2008, **18**(15), 2205–2214.
37 B. Chen, N. W. Ockwig, A. R. Millward, D. S. Contreras and O. M. Yaghi, High H_2 adsorption in a microporous metal-organic framework with open metal sites, *Angew. Chem., Int. Ed.*, 2005, **44**(30), 4745–4749.
38 X. Lin, I. Telepeni, A. J. Blake, A. Dailly, C. M. Brown, J. M. Simmons, M. Zoppi, G. S. Walker, K. M. Thomas, T. J. Mays, P. Hubberstey, N. R. Champness and M. Schroder, High capacity hydrogen adsorption in Cu (II) tetracarboxylate framework materials: the role of pore size, ligand functionalization, and exposed metal sites, *J. Am. Chem. Soc.*, 2009, **131**(6), 2159–2171.
39 D. Chakraborty, S. Nandi, R. Maity, R. K. Motkuri, K. S. Han, S. Collins, P. Humble, J. C. Hayes, T. K. Woo, R. Vaidhyanathan and P. K. Thallapally, An ultra-microporous metal–organic framework with exceptional xe capacity, *Chem. – Eur. J.*, 2020, **26**(55), 12544–12548.
40 T. Tozawa, J. T. A. Jones, S. I. Swamy, S. Jiang, D. J. Adams, S. Shakespeare, R. Clowes, D. Bradshaw, T. Hasell, S. Y. Chong, C. Tang, S. Thompson, J. Parker, A. Trewin, J. Bacsa, A. M. Z. Slawin, A. Steiner and A. I. Cooper, Porous organic cages, *Nat. Mater.*, 2009, **8**(12), 973–978.
41 H. Wang, K. Yao, Z. Zhang, J. Jagiello, Q. Gong, Y. Han and J. Li, The first example of commensurate adsorption of atomic gas in a mof and effective separation of xenon from other noble gases, *Chem. Sci.*, 2014, **5**(2), 620–624.
42 J. J. Perry IV, S. L. Teich-McGoldrick, S. T. Meek, J. A. Greathouse, M. Haranczyk and M. D. Allendorf, Noble gas adsorption in metal-organic frameworks containing open metal sites, *J. Phys. Chem. C*, 2014, **118**(22), 11685–11698.

43 L. Chen, P. S. Reiss, S. Y. Chong, D. Holden, K. E. Jelfs, T. Hasell, M. A. Little, A. Kewley, M. E. Briggs, A. Stephenson, K. M. Thomas, J. A. Armstrong, J. Bell, J. Busto, R. Noel, J. Liu, D. M. Strachan, P. K. Thallapally and A. I. Cooper, Separation of rare gases and chiral molecules by selective binding in porous organic cages, *Nature Materials*, 2014, **13**(10), 954–960.

44 P. K. Thallapally, J. W. Grate and R. K. Motkuri, Facile xenon capture and release at room temperature using a metal-organic framework: a comparison with activated charcoal, *Chem. Commun.*, 2012, **48**(3), 347–349.

45 AquaCarb and Westates. Westates® coconut shell based granular activated carbon - aquacarb® 830c, 1230c and 1240c carbons. https://www.evoqua.com/siteassets/documents/products/carbon-resin/wsaq12ds.pdf, 2017.

46 S. T. Meek, S. L. Teich-McGoldrick, J. J. Perry, J. A. Greathouse and M. D. Allendorf, Effects of polarizability on the adsorption of noble gases at low pressures in monohalogenated isoreticular metal-organic frameworks, *J. Phys. Chem. C*, 2012, **116**(37), 19765–19772.

47 D. Dubbeldam, S. Calero, D. E. Ellis and R. Q. Snurr, RASPA: molecular simulation software for adsorption and diffusion in flexible nanoporous materials, *Mol. Simul.*, 2015, **42**(2), 81–101.

48 D. Dubbeldam, S. Calero and T. J. H. Vlugt, iRASPA: GPU-accelerated visualization software for materials scientists, *Mol. Simul.*, 2018, **44**(8), 653–676.

49 A. Ahmed, S. Seth, J. Purewal, A. G. Wong-Foy, M. Veenstra, A. J. Matzger and D. J. Siegel, Exceptional hydrogen storage achieved by screening nearly half a million metal-organic frameworks, *Nat. Commun.*, 2019, **10**(1), 1568.

50 C. E. Wilmer, M. Leaf, C. Yeon Lee, O. K. Farha, B. G. Hauser, J. T. Hupp and R. Q. Snurr, Large-scale screening of hypothetical metal–organic frameworks, *Nat. Chem.*, 2011, **4**(2), 83–89.

51 C. D. Wood, B. Tan, A. Trewin, F. Su, M. J. Rosseinsky, D. Bradshaw, Y. Sun, L. Zhou and A. I. Cooper, Microporous organic polymers for methane storage, *Adv. Mater.*, 2008, **20**(10), 1916–1921.

52 P. Z. Moghadam, A. Li, S. B. Wiggin, A. Tao, A. G. P. Maloney, P. A. Wood, S. C. Ward and D. Fairen-Jimenez, Development of a cambridge structural database subset: a collection of metal–organic frameworks for past, present, and future, *Chem. Mater.*, 2017, **29**(7), 2618–2625.

53 Y. G. Chung, E. Haldoupis, B. J. Bucior, M. Haranczyk, S. Lee, H. Zhang, K. D. Vogiatzis, M. Milisavljevic, S. Ling, J. S. Camp, B. Slater, J. I. Siepmann, D. S. Sholl and R. Q. Snurr., Advances, updates, and analytics for the computation-ready, experimental metal–organic framework database: CoRE MOF 2019, *J. Chem. Eng. Data*, 2019, **64**(12), 5985–5998.

54 M. Kezirian, K. Johnson and S. Phoenix, Composite overwrapped pressure vessels (COPV): Flight rationale for the Space Shuttle Program, In *American Institute of Aeronautics and Astronautics Space 2011 Conference & Exposition*, page 7363, 2011.

55 W. Radtke, Manufacturing of advanced titanium (lined) propellant tanks and high pressure vessels. Proceedings of the 4th International Spacecraft Propulsion Conference (ESA SP-555), 2004.

56 P. García-Holley, B. Schweitzer, T. Islamoglu, Y. Liu, L. Lin, S. Rodriguez, M. H. Weston, J. T. Hupp, D. A. Gómez-Gualdrón, T. Yildirim and O. K. Farha, Benchmark study of hydrogen storage in metal–organic frameworks under temperature and pressure swing conditions, *ACS Energy Lett.*, 2018, **3**(3), 748–754.

57 J. A. Mason, M. Veenstra and J. R. Long, Evaluating metal-organic frameworks for natural gas storage, *Chem. Sci.*, 2014, **5**(1), 32–51.

58 A. Sturluson, M. T. Huynh, A. R. Kaija, C. Laird, S. Yoon, F. Hou, Z. Feng, C. E. Wilmer, Y. J. Colón, Y. G. Chung, D. Siderius and C. Simon, The role of molecular modelling and simulation in the discovery and deployment of metal-organic frameworks for gas storage and separation, *Mol. Simul.*, 2019, **45**(14–15), 1082–1121.

59 H. Daglar and S. Keskin, Recent advances, opportunities, and challenges in high-throughput computational screening of MOFs for gas separations, *Coord. Chem. Rev.*, 2020, **422**, 213470.

60 P. G. Boyd, Y. Lee and B. Smit, Computational development of the nanoporous materials genome, *Nat. Rev. Mater.*, 2017, **2**(8), 17037.